

Photon noise from chaotic and coherent millimeter-wave sources measured with horn-coupled, aluminum lumped-element kinetic inductance detectors

D. Flanigan,^{1, a)} H. McCarrick,¹ G. Jones,¹ B. R. Johnson,¹ P. Ade,² D. Araujo,¹ K. Bradford,³ R. Cantor,⁴ G. Che,⁵ P. Day,⁶ S. Doyle,² C. B. Kjellstrand,¹ H. Leduc,⁶ M. Limon,¹ V. Luu,¹ P. Mauskopf,^{2,3,5} A. Miller,¹ T. Mroczkowski,⁷ C. Tucker,² and J. Zmuidzinas^{6,8}

¹⁾Department of Physics, Columbia University, New York, NY 10027, USA

²⁾School of Physics and Astronomy, Cardiff University, Cardiff, Wales CF24 3AA, UK

³⁾School of Earth and Space Exploration, Arizona State University, Tempe, AZ 85287, USA

⁴⁾STAR Cryoelectronics, Santa Fe, NM 87508, USA

⁵⁾Department of Physics, Arizona State University, Tempe, AZ 85287, USA

⁶⁾Jet Propulsion Laboratory, Pasadena, CA 91109, USA

⁷⁾Naval Research Laboratory, Washington, DC 20375, USA

⁸⁾Division of Physics, Mathematics, and Astronomy, California Institute of Technology, Pasadena, CA 91125, USA

(Dated: 23 October 2015)

We report photon-noise limited performance of horn-coupled, aluminum lumped-element kinetic inductance detectors at millimeter wavelengths. The detectors are illuminated by a millimeter-wave source that uses an active multiplier chain to produce radiation between 140 and 160 GHz. We feed the multiplier with either amplified broadband noise or a continuous-wave tone from a microwave signal generator. We demonstrate that the detector response over a 40 dB range of source power is well-described by a simple model that considers the number of quasiparticles. The detector noise-equivalent power (NEP) is dominated by photon noise when the absorbed power is greater than approximately 1 pW, which corresponds to $\text{NEP} \approx 2 \times 10^{-17} \text{ W Hz}^{-1/2}$, referenced to absorbed power. At higher source power levels we observe the relationships between noise and power expected from the photon statistics of the source signal: $\text{NEP} \propto P$ for broadband (chaotic) illumination and $\text{NEP} \propto P^{1/2}$ for continuous-wave (coherent) illumination. We develop a detailed model for the device noise and demonstrate absolute calibration of the absorbed power in both source modes using the scaling of the photon noise with power.

A kinetic inductance detector¹ (KID) is a thin-film superconducting resonator designed to detect photons that break Cooper pairs. This detector technology is being developed for a range of applications across the electromagnetic spectrum. Our devices are being developed for cosmic microwave background (CMB) studies.

The randomness of photon arrivals sets the fundamental sensitivity limit for radiation detection. In recent years, several groups have used spectrally-filtered thermal sources to perform laboratory measurements of both aluminum and titanium nitride KIDs that demonstrate sensitivity limited by photon noise.^{2–6} Here, we use an electronic source to demonstrate photon-noise limited performance of horn-coupled, aluminum lumped-element kinetic inductance detectors^{7,8} (LEKIDs) sensitive to a 40 GHz spectral band centered on 150 GHz.

The array of devices used in this study was fabricated by patterning a 20 nm aluminum film on a high-resistivity crystalline silicon substrate, with twenty detectors per array. Each resonator comprises lithographed structures that behave electrically as lumped elements, namely an interdigitated capacitor and an inductive meander that is also the photon absorber. Schematics of a detector and the horn coupling scheme are shown in Figure 1. These devices were fabricated at STAR Cryoelectronics⁹ using the same lithographic mask used to pattern the devices described in a previous study.¹⁰ The same processing steps were used in this study except that the silicon wafer was immersed in hydrofluoric acid prior to alu-

minum deposition in order to clean and hydrogen-terminate the silicon surface to reduce oxide formation. We measure a superconducting transition temperature $T_c = 1.39 \text{ K}$. The resonance frequencies are $95 \text{ MHz} < f_r < 195 \text{ MHz}$. Under the lowest loading conditions the internal quality factors are $Q_i \approx 5 \times 10^5$. The coupling quality factors are $Q_c \approx 5 \times 10^4$. The detector bath temperature is $120 \pm 1 \text{ mK}$, obtained in a cryostat using an adiabatic demagnetization refrigerator backed by a helium pulse tube cooler. Detector readout is performed with a homodyne system using a cryogenic SiGe low-noise amplifier and open-source digital signal-processing hardware.^{10,11} All the data shown are from a single representative detector with $f_r = 164 \text{ MHz}$, and were taken at a constant readout tone power of approximately -100 dBm on the feedline. The package that contains the detector chip is machined from QC-10, which is an aluminum alloy known to superconduct at the bath temperature used here.

Figure 1(a) is a schematic of the millimeter-wave source, located outside the cryostat. Within the source, the output of a $12 \times$ active multiplier chain passes through two variable waveguide attenuators that allow the output power to be controlled over a range of more than 50 dB. The primary components of the source are listed in the Supplemental Material.¹²

The output spectrum is controlled by a band-pass filter with a sharp roll-off outside its passband of 140 to 160 GHz. Within this passband, the source can produce radiation in two modes. In *broadband* mode, amplified noise is multiplied into a broadband chaotic signal. In *continuous-wave* mode, a multiplied tone from a signal generator approximates a monochromatic coherent signal. We have measured the source output

^{a)}Electronic mail: daniel.flanigan@columbia.edu

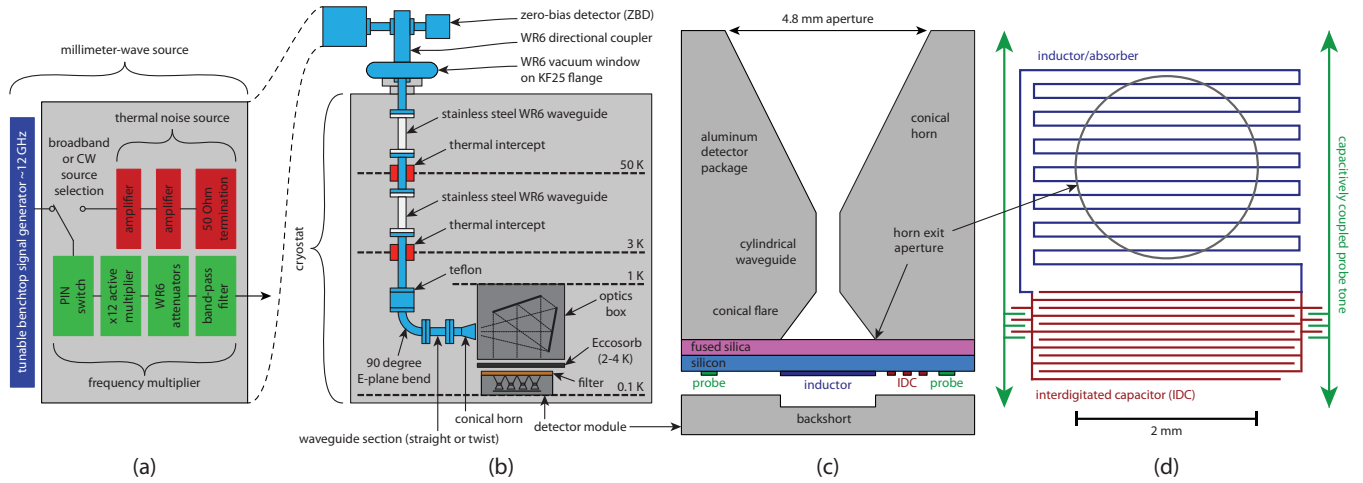


FIG. 1. Experiment schematics. **(a)** The millimeter-wave source components. **(b)** The source and cryogenic setup. **(c)** A cross-section of an array element. The inner conical flare and fused silica layer are designed for impedance matching. **(d)** The lumped circuit elements of one LEKID. Parts of this figure are reproduced with permission from H. McCarrick *et al.*, *Rev. Sci. Instrum.* **85**, 123117 ©2014 American Institute of Physics.

in both modes using a Fourier transform spectrometer; these measurements show that in broadband mode the power is constant within a factor of two across the output band, and in continuous-wave mode it appears monochromatic with negligible higher harmonics.

Figure 1(b) shows the signal path from the source through the cryostat to the detectors. The source output is split using a waveguide directional coupler that sends 99% of the power into a calibrated, isolator-coupled zero-bias diode power detector (ZBD), the voltage output of which is recorded using a lock-in amplifier. The remaining 1% of the power travels through a vacuum window and into the cryostat through WR6 waveguide. A piece of Teflon at 4 K inserted into the waveguide absorbs room-temperature thermal radiation. Two mirrors transform the output of a conical horn into a collimated beam. A 6.4 mm thick slab of microwave absorber (Eccosorb MF-110), regulated at 2 K during these measurements, attenuates incoming signals and provides a stable background load. A metal-mesh filter at the detector apertures defines the upper edge of the detector band at 170 GHz. The lower edge of the band at 130 GHz is defined by the cutoff frequency of a 1.35 mm diameter circular waveguide in the detector package. We note that the source output is within the single-mode bandwidth of both WR6 waveguide and the circular waveguide. The radiation from the source incident on the detector horns is linearly polarized, and the electric field is aligned with the long elements of the inductive meanders in the detectors.

Figure 2 shows the main results of this work. All power values in this figure refer to the power from the source absorbed by the detector: $P_A = \eta_S P_S$, where P_S is measured by the ZBD. Before calibration, the efficiency η_S is known only approximately from measurements and simulations of the components between the source and the detector. We accurately determine η_S , and thus the absorbed power, by measuring the relationship between source power and detector noise. This absolute calibration relies on the assumption that all compo-

nents between the source output and detector are linear: we have linearized the ZBD response at the higher power levels, and all other components are passive. To perform the absolute calibration we use measurements of the noise-equivalent power (NEP), defined as the standard error of the mean in the inferred optical power at a given point in the optical system after 0.5 s of integration.^{13,14} We calculate the NEP using measurements of the detector noise and responsivity.

At each source power and readout power level, to determine the resonance frequency and the quality factors, we sweep the readout tone generator frequency f_g across a resonance and fit a resonator model to the forward scattering parameter $S_{21}(f_g)$ data.¹⁰ Figure 2(c) shows the detector response to source power in both broadband and continuous-wave modes. At low source power in both modes the fractional frequency shift $x(P_A) = f_r(0)/f_r(P_A) - 1$ is approximately linear in power, while at high power $x \propto P_A^{1/2}$. This behavior is described by a model in which the fractional frequency shift is proportional to the number of quasiparticles:

$$N_{qp} = N_* \left[(1 + 2\tau_{\max}\Gamma/N_*)^{1/2} - 1 \right], \quad (1)$$

where $\Gamma \propto P_A$ is the rate of quasiparticle generation and N_* and τ_{\max} are material-dependent constants.¹⁵ We calculate the responsivity dx/dP_S at each source power level with a finite-difference derivative that uses the fractional frequency response at adjacent power levels.

To measure detector noise we record time-ordered data $S_{21}(f_g = f_r)$. Using the resonator model from the fit to the frequency sweep we convert these data into units of fractional frequency shift x , then calculate the single-sided spectral density $S_x(f)$. Figures 2(a) and 2(b) show the measured noise spectra and fits to the following model:

$$S_x(f) = \frac{W^2}{1 + (2\pi f\tau)^2} + A^2, \quad (2)$$

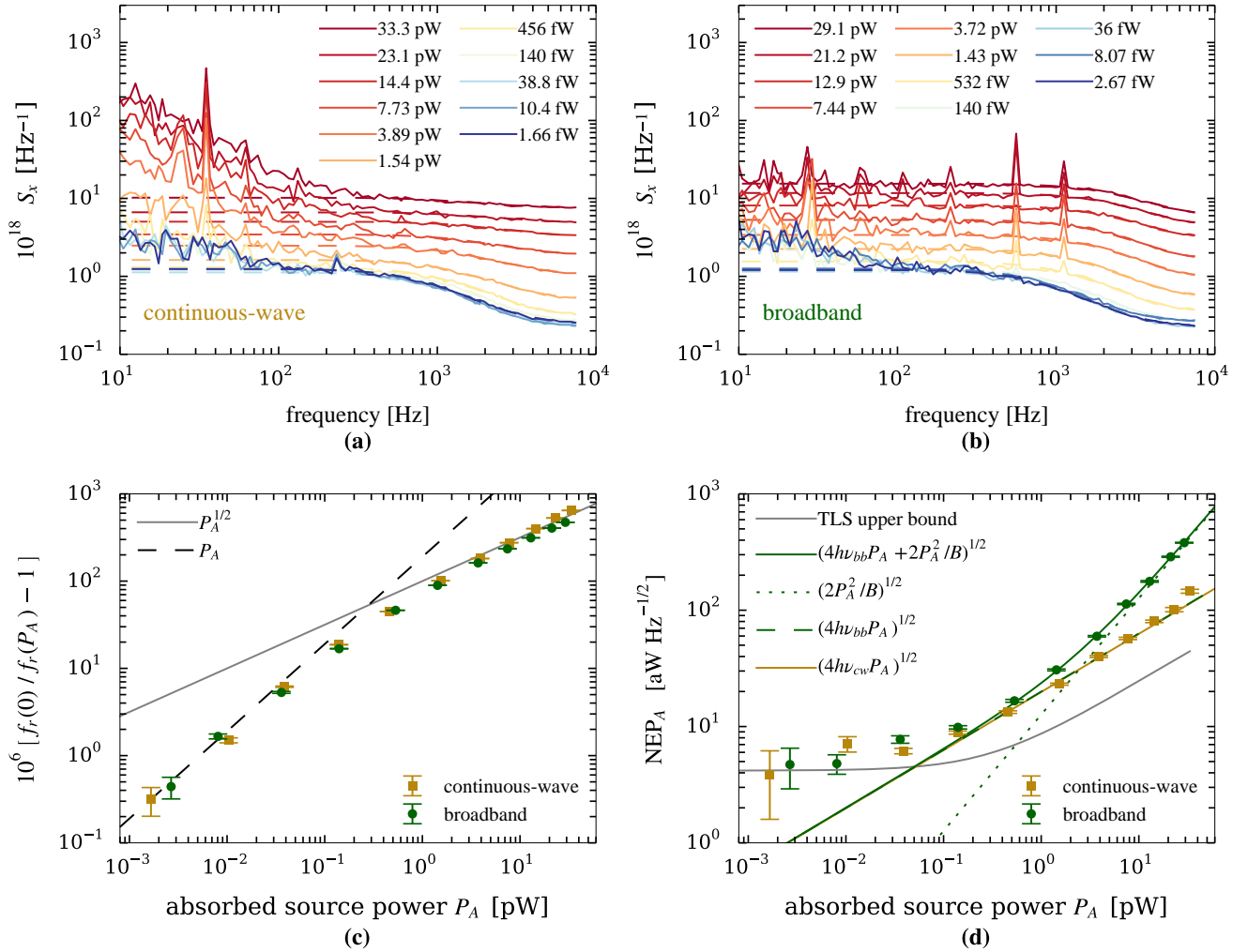


FIG. 2. Primary results of the experiment. **(a)** Spectral density S_x of detector time-ordered data versus frequency under continuous-wave $\nu_{cw} = 148$ GHz illumination (solid lines), and the result of fitting the data to Equation 2 (dashed lines). At high power the red noise component is dominated by fluctuations from the signal generator that feeds the multiplier; these fluctuations are correlated among detectors. **(b)** Spectral density under broadband illumination, and fits of Equation 2. The spikes above 400 Hz are pickup from a fan in the source, and are masked when fitting the data. The red noise present below 100 Hz at low source power in both modes is produced by vibrations from the pulse tube cooler that vanish when it is turned off. To reduce bias due to low-frequency noise contributions we fit only to the data above 100 Hz. The detector white noise levels from the fits are used to calculate NEP values. **(c)** Fractional frequency response versus absorbed power in both source modes. The error bars are statistical errors from the resonator fits. The finite-difference derivative of these response data are used to calculate the NEP. The dashed black line and solid gray line are guides that show how the response scales at both low and high absorbed power. **(d)** Noise-equivalent power versus absorbed power in both source modes. All data points and lines are referenced to absorbed power. The error bars are propagated statistical errors from the finite difference derivative dx/dP_A and the detector noise fits. The solid green line is the sum of the quadratic and linear terms in the fit of Equation 6 to the broadband NEP 2 data. The dotted green line is the quadratic term, which is the photon wave noise contribution. The dashed green line is the linear term, which contains equal contributions from photon shot noise and quasiparticle recombination noise. The broadband frequency used is $\nu_{bb} = 150$ GHz, near the band center. The solid brown line (nearly coincident with dashed green) is the linear term in the fit of Equation 6 to the continuous-wave NEP 2 data, in which the quadratic term is omitted. The solid gray line is a conservative upper bound on the NEP contribution of two-level system noise that is derived in the Supplemental Material.¹² The labels in (a) and (b) as well as the horizontal axes in (c) and (d) show absorbed power $P_A = \eta_S P_S$, where P_S is measured power at the source output and $\eta_S \sim 10^{-6}$ is obtained in each source mode by fitting the corresponding NEP data.

where the free parameters are the detector white noise W^2 , the amplifier white noise A^2 , and the time constant τ . The detector audio bandwidth of about 1 kHz corresponds to a limiting time constant τ that is approximately equal to both the res-

onator ring-down time $\tau_r = Q/\pi f_r$ and the expected quasiparticle relaxation time τ_{qp} for aluminum.

To model the detector noise, we first consider noise sources independent of the quasiparticle system. White noise due to

the cryogenic amplifier dominates at frequencies well above the detector bandwidth, and we account for it in the noise spectra model. Two-level systems (TLS) in amorphous dielectric surface layers located near the resonator produce fluctuations in the local dielectric constant and thus in f_r .¹⁶ To measure the TLS noise contribution we performed a separate experiment with the horn apertures covered by aluminum tape and a low readout tone power. Under these conditions, the TLS contribution is increased and quasiparticle generation from optical and readout photons is decreased. The analysis of this experiment is described in the Supplemental Material,¹² and a conservative upper bound on the TLS contribution to the NEP is shown in Figure 2(d). Because this upper bound shows that TLS noise is negligible at high source power, we do not model it as a function of absorbed power.

The remaining noise sources involve fluctuations in the quasiparticle system: generation by optical photons, readout photons, and thermal phonons, as well as quasiparticle recombination, e.g. via phonon emission. All of these sources are expected to produce white noise that rolls off at the frequency corresponding to the larger of τ_r and τ_{qp} .¹⁵ We expect readout generation to be negligible at high source power, and treat it as constant. (Where present, the photon wave noise introduces correlations between photon arrival times. This noise has a bandwidth equal to the 20 GHz bandwidth of the absorbed broadband radiation, so it is also expected to appear white in the detector audio band.¹⁷)

The NEP model includes theoretical expectations for photon noise and quasiparticle recombination noise. We denote by n the mean photon occupancy of a single spatial/polarization mode of the electromagnetic field with frequency ν . For example, for a thermal source at temperature T the occupancy is $n = [\exp(h\nu/k_B T) - 1]^{-1}$, where h is Planck's constant and k_B is Boltzmann's constant. If we assume that the radiation occupies an optical bandwidth $B \ll \nu$ sufficiently narrow that quantities such as occupancy and absorption efficiency can be treated as constant, then the power from this mode that is absorbed by a detector with absorption efficiency η is $P_A = \eta n B h \nu$. If the source is thermal then the contribution of photon noise to the NEP is given by¹⁴

$$\text{NEP}_{A,\gamma}^2 = 2\eta n(1 + \eta n)B(h\nu)^2 = 2h\nu P_A + 2P_A^2/B, \quad (3)$$

which is referenced to absorbed power. We refer respectively to these two terms as shot noise and wave noise, following Hanbury Brown and Twiss.¹⁸ If the source is monochromatic with perfect temporal coherence then only the shot noise term is present regardless of the occupancy: this behavior represents a key difference between a quantum coherent state and a quantum-statistical thermal state of the field.^{19,20} For a thermal source, if $\eta n \ll 1$ the shot noise dominates, which is typical in optical astronomy; if $\eta n \gg 1$ the wave noise dominates, which is typical in radio astronomy.

We measure power at the output of the source and detector NEP referenced to the same point. Referencing the photon NEP to the source output gives

$$\text{NEP}_{S,\gamma}^2 = \text{NEP}_{A,\gamma}^2/\eta_S^2 = 2h\nu P_S/\eta_S + 2P_S^2/B. \quad (4)$$

The presence of the efficiency η_S in the linear term of this equation enables the absolute calibration.

Previous studies that calculated the absorption efficiency of a KID by measuring the scaling of photon shot noise with optical power have used superconducting films with transition temperatures similar to the film used here but much larger photon energies.^{2,3,5,6} Here, the photons have energies $h\nu \gtrsim 2\Delta$, where Δ is the superconducting energy gap, so each photon excites only two quasiparticles close to the gap, and in this limit the quasiparticle recombination noise is significant. As derived in the Supplemental Material,¹² the recombination noise contribution to NEP_A is

$$\text{NEP}_{A,R}^2 = 4\Delta P_A/\eta_{pb} \quad (5)$$

where η_{pb} is the pair-breaking efficiency. For photon energies $2\Delta < h\nu < 4\Delta$, a recent measurement found $\eta_{pb} \approx 2\Delta/h\nu$, in agreement with theory.²¹ Using this value, the recombination NEP equals the shot noise term in the photon NEP. This is expected based on the symmetry between uncorrelated pair-breaking events and uncorrelated pair-recombination events.

Finally, we introduce a small constant term NEP_0 to account for noise sources independent of source power, such as TLS noise and quasiparticle generation-recombination noise from thermal phonons, readout photons, and ambient photons.

To calculate the measured detector NEP we divide the white noise component W , obtained from fits of Equation 2 to $S_x(f)$, by the responsivity to source power: $\text{NEP}_S = W/(dx/dP_S)$. We compare this to the model for the source-referenced detector NEP:

$$\begin{aligned} \text{NEP}_S^2 &= (\text{NEP}_{A,0}^2 + \text{NEP}_{A,R}^2 + \text{NEP}_{A,\gamma}^2)/\eta_S^2 \\ &= \text{NEP}_{A,0}^2/\eta_S^2 + [2(2h\nu P_A) + 2P_A^2/B]/\eta_S^2 \\ &= \text{NEP}_{S,0}^2 + 4h\nu P_S/\eta_S + 2P_S^2/B. \end{aligned} \quad (6)$$

The right-hand side is a quadratic in P_S with unknown quantities $\text{NEP}_{S,0}$, η_S , and B . We fit a quadratic to the broadband data using center frequency $\nu_{bb} = 150$ GHz and obtain $\eta_S = 8.15 \times 10^{-7} (1 \pm 0.08)$. The quadratic coefficient implies an effective bandwidth $B = 12$ GHz. The quadratic term is not expected to be present for coherent illumination, so we fit a line to the continuous-wave data using $\nu_{cw} = 148$ GHz and obtain $\eta_S = 8.93 \times 10^{-7} (1 \pm 0.06)$.

Figure 2(d) is a plot of NEP_A that shows that photon noise dominates when $P_A \gtrsim 1$ pW, which corresponds to $\text{NEP}_A \approx 2 \times 10^{-17}$ W Hz^{-1/2}. At high power in each source mode we observe the expected relationship between noise and power: in broadband mode $\text{NEP} \propto P$ because the quadratic wave noise term dominates, while in continuous-wave mode $\text{NEP} \propto P^{1/2}$ because the quadratic term is not present. This behavior is a clear signature of photon noise.

Analysis of data from twelve detectors yielded similar results to those shown in Figure 2(d), with the photon noise starting to dominate between 0.5 and 1 pW. We conclude that these detectors become limited by photon noise at absorbed power levels lower than the background power levels already measured by ground-based CMB polarimeters.^{22,23}

R. C. is both an author and the owner of STAR Cryoelectronics. H. M. is supported by a NASA Earth and Space Sciences Fellowship. T. M. is supported by a National Research Council Fellowship. This research is supported in part by a grant from the Research Initiatives for Science and Engineering program at Columbia University to B. R. J., and by internal Columbia University funding to A. M. We thank the Xilinx University Program for their donation of FPGA hardware and software tools used in the readout system.

- ¹P. K. Day, H. G. LeDuc, B. A. Mazin, A. Vayonakis, and J. Zmuidzin, *Nature* **425**, 817 (2003).
- ²S. J. C. Yates, J. J. A. Baselmans, A. Endo, R. M. J. Janssen, L. Ferrari, P. Diener, and A. M. Baryshev, *Appl. Phys. Lett.* **99**, 073505 (2011).
- ³R. M. J. Janssen, J. J. A. Baselmans, A. Endo, L. Ferrari, S. J. C. Yates, A. M. Baryshev, and T. M. Klapwijk, *Appl. Phys. Lett.* **103**, 203503 (2013).
- ⁴P. D. Mauskopf, S. Doyle, P. Barry, S. Rowe, A. Bidead, P. A. R. Ade, C. Tucker, E. Castillo, A. Monfardini, J. Goupy, and M. Calvo, *J. Low Temp. Phys.* **176**, 545 (2014).
- ⁵P. de Visser, J. J. A. Baselmans, J. Bueno, N. Llombart, and T. M. Klapwijk, *Nat. Commun.* **5**, 3130 (2014).
- ⁶J. Hubmayr, J. Beall, D. Becker, H.-M. Cho, M. J. Devlin, B. Dober, C. Groppi, G. C. Hilton, K. D. Irwin, D. Li, P. Mauskopf, D. P. Pappas, J. Van Lanen, M. R. Vissers, Y. Wang, L. F. Wei, and J. Gao, *Appl. Phys. Lett.* **106**, 073505 (2015).
- ⁷S. Doyle, Ph.D. thesis, Cardiff University (2008).
- ⁸S. Doyle, P. Mauskopf, J. Zhang, A. Monfardini, L. J. Swenson, J. J. A. Baselmans, S. J. C. Yates, and M. Roesch, *Proc. SPIE* **7741**, 77410M (2010).
- ⁹See <http://www.starcryo.com> for information about STAR Cryoelectronics.
- ¹⁰H. McCarrick, D. Flanigan, G. Jones, B. R. Johnson, P. A. R. Ade, D. Araujo, K. Bradford, R. Cantor, G. Che, P. Day, S. Doyle, H. G. LeDuc, M. Limon, V. Luu, P. Mauskopf, A. Miller, T. Mroczkowski, C. Tucker, and J. Zmuidzin, *Rev. Sci. Instrum.* **85**, 123117 (2014).
- ¹¹See <http://www.github.com/ColumbiaCMB> for the software used to read out the detectors and analyze the data.
- ¹²See supplemental material at [URL will be inserted by AIP] for a list of the millimeter-wave source components and more detailed analysis of TLS noise and recombination noise.
- ¹³P. L. Richards, *J. Appl. Phys.* **76**, 1 (1994).
- ¹⁴J. Zmuidzin, *Appl. Opt.* **42**, 4989 (2003).
- ¹⁵J. Zmuidzin, *Annu. Rev. Condens. Matter Phys.* **3**, 169 (2012).
- ¹⁶J. Gao, M. Daal, J. M. Martinis, A. Vayonakis, J. Zmuidzin, B. Sadoulet, B. A. Mazin, P. K. Day, and H. G. LeDuc, *Appl. Phys. Lett.* **92**, 212504 (2008).
- ¹⁷J. Zmuidzin, accepted for publication in *ApJ* (2015), arXiv:1501.03219v2.
- ¹⁸R. Hanbury Brown and R. Q. Twiss, *Proc. R. Soc. A* **242**, 300 (1957).
- ¹⁹R. Loudon, *The Quantum Theory of Light; 3rd ed.* (Oxford Univ. Press, Oxford, 2002).
- ²⁰R. J. Glauber, “Nobel Lecture: One Hundred Years of Light Quanta,” <http://www.nobelprize.org/nobel_prizes/physics/laureates/2005/glauber-lecture.html>.
- ²¹P. de Visser, S. J. C. Yates, T. Guruswamy, D. J. Goldie, S. Withington, A. Neto, N. Llombart, A. M. Baryshev, T. M. Klapwijk, and J. J. A. Baselmans, *Appl. Phys. Lett.* **106**, 252602 (2015).
- ²²E. M. George, P. A. R. Ade, K. A. Aird, J. E. Austermann, J. A. Beall, D. Becker, A. N. Bender, B. A. Benson, L. E. Bleem, J. Britton, J. E. Carlstrom, C. L. Chang, H. C. Chiang, H.-M. Cho, T. M. Crawford, A. T. Crites, A. Datsman, T. de Haan, M. A. Dobbs, W. Everett, A. Ewall-Wice, N. W. Halverson, N. Harrington, J. W. Henning, G. C. Hilton, W. L. Holzapfel, S. Hoover, N. Huang, J. Hubmayr, K. D. Irwin, M. Karfinkle, R. Keisler, J. Kennedy, A. T. Lee, E. Leitch, D. Li, M. Lueker, D. P. Marrone, J. J. McMahon, J. Mehl, S. S. Meyer, J. Montgomery, T. E. Montroy, J. Nagy, T. Natoli, J. P. Nibarger, M. D. Niemack, V. Novosad, S. Padin, C. Pryke, C. L. Reichardt, J. E. Ruhl, B. R. Saliwanchik, J. T. Sayre, K. K. Schaffer, E. Shirokoff, K. Story, C. Tucker, K. Vanderlinde, J. D. Vieira, G. Wang, R. Williamson, V. Yefremenko, K. W. Yoon, and E. Young, *Proc. SPIE* **8452**, 84521F (2012).
- ²³Bicep2 Collaboration, P. A. R. Ade, R. W. Aikin, M. Amiri, D. Barkats, S. J. Benton, C. A. Bischoff, J. J. A. P. Bock, J. A. Brevik, I. Buder, E. Bullock, G. Davis, P. K. Day, C. D. Dowell, L. Duband, J. P. Filippini, S. Fliesch, S. R. Golwala, M. Halpern, M. Hasselfield, S. R. Hildebrandt, G. C. Hilton, K. D. Irwin, K. S. Karkare, J. P. Kaufman, B. G. Keating, S. A. Kernasovskiy, J. M. Kovac, C. L. Kuo, E. M. Leitch, N. Llombart, M. Lueker, C. B. Netterfield, H. T. Nguyen, R. O’Brien, R. W. Ogburn IV, A. Orlando, C. Pryke, C. D. Reintsema, S. Richter, R. Schwarz, C. D. Sheehy, Z. K. Staniszewski, K. T. Story, R. V. Sudiwala, G. P. Teply, J. E. Tolan, A. D. Turner, A. G. Viereg, P. Wilson, C. L. Wong, and K. W. Yoon, *ApJ* **792**, 62 (2014).
- ²⁴J. Gao, J. Zmuidzin, B. A. Mazin, H. G. LeDuc, and P. K. Day, *Appl. Phys. Lett.* **90**, 102507 (2007).
- ²⁵R. Barends, N. Verbruggen, A. Endo, P. de Visser, T. Zijlstra, T. M. Klapwijk, and J. J. A. Baselmans, *Appl. Phys. Lett.* **97**, 033507 (2010).
- ²⁶C. Neill, A. Megrant, R. Barends, Y. Chen, B. Chiaro, J. Kelly, J. Y. Mutus, P. J. J. O’Malley, D. Sank, J. Wenner, T. C. White, Y. Yin, A. N. Cleland, and J. M. Martinis, *Appl. Phys. Lett.* **103**, 072601 (2013).

SUPPLEMENTAL MATERIAL

Millimeter-wave source

Component	Vendor	Part Number
50 Ω terminator	Minicircuits	ANNE-50X
High gain amplifiers	Spacek Labs	SG134-40-17
PIN switch	Narda	S213D
Active multiplier	Millitech	AMC-05
Variable attenuators	Custom Microwave	VA6R
Band-pass filter	Pacific Millimeter	14020
Directional coupler	Millitech	CL3-006
Zero-bias diode power detector	Virginia Diodes, Inc.	WR6.5-ZBD

TABLE S1. Primary components of the millimeter-wave source.

Two-level system noise

At low temperatures we see evidence for two-level system (TLS) effects in measurements of resonance frequency versus bath temperature, which depart from the Mattis-Bardeen prediction, and in the fact that the internal quality factors increase with increasing readout power. The connection between these static TLS effects and TLS noise is not fully understood. The method we used to estimate the TLS noise contribution is described in this section.

In this work, the motivation for modeling TLS noise is that the detector responsivity decreases with increased optical loading: as shown in Figure 2(c), at high power $x(P_S) \propto P_S^{1/2}$, so the responsivity $dx/dP_S \propto P_S^{-1/2}$. Thus, a noise source with constant amplitude W^2 in fractional frequency units would be linear and increasing with power when converted to NEP units:

$$\text{NEP}^2 = W^2(dx/dP_S)^{-2} \propto W^2 P$$

The presence of such a noise source would complicate the extraction of the linear NEP term.

The TLS contribution to the spectral density is typically

$$S_{x,\text{TLS}}(f, P_i) \propto f^{-1/2}(1 + P_i/P_*)^{-1/2},$$

where P_i is the absorbed readout power and the critical power P_* is small compared to the readout power levels typically used with KIDs.^{15,16,24–26} The experiment described in the main text is performed with constant P_g , and we expect the TLS noise level to vary as $P_i^{-1/2} = (\chi_a P_g)^{-1/2}$, where $\chi_a \leq 1/2$ can be calculated from resonator parameters.¹⁵

In order to set an upper bound on the TLS contribution to the NEP, we performed a separate experiment in which we attempted to make any TLS noise as prominent as possible. Three key aspects differ from the experiment described in the main text: the horn apertures were covered with aluminum

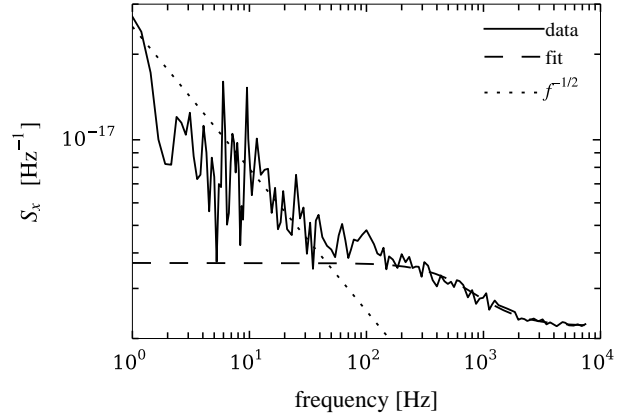


FIG. S1. Dark noise data for the same detector characterized in the main text. The solid line is the data, the dashed line is a fit to the same noise model used in the main text, and the dotted line is a guide that is proportional to $f^{-1/2}$, which is the expected behavior of TLS noise.

tape to minimize optical loading; the readout power was approximately -112 dBm, 12 dB lower than in the primary experiment; in order to remove noise due to vibrations caused by the pulse tube cooler, we turned it off to record time-ordered data while the adiabatic demagnetization refrigerator continued to regulate the bath temperature at 120 mK.

Figure S1 shows the fractional frequency spectral density taken under these dark conditions. The dashed line shows a fit to the same model used in the main text. The dotted line is a guide, intended to indicate a possible TLS contribution, that goes as $f^{-1/2}$. To place an upper bound on the TLS contribution we use the white noise level W_{dark}^2 from this fit, scale it by the change in internal readout power, and convert this to NEP:

$$\text{NEP}_{S,\text{TLS}}^2 = W_{\text{dark}}^2 (P_{i,\text{dark}}/P_i)^{1/2} (dx/dP_S)^{-2}.$$

This is conservative because the TLS noise spectral density is falling with frequency so the actual contribution is likely to be much lower; recall that the noise fits in the main text use only data at frequencies above 100 Hz.

The TLS upper bound shown in Figure 2(d) is a polynomial fit to the derived NEP_{TLS} values for the continuous-wave data set. We see that the calculated TLS contribution does increase as the responsivity decreases, but the increase is sub-linear because the absorbed readout power increases as the internal and coupling quality factors become better matched at higher source power levels. Even at the level of the upper bound, at higher source powers TLS noise does not contribute significantly to the NEP, so modeling it in detail would unnecessarily complicate the model fitting procedure without affecting the result.

Recombination noise

In this section we derive from first principles Equation 5 in the main text because it differs by a factor of two from ex-

pressions that have appeared in the literature.^{2,3,5,6,10} Consider a flow of quanta q at rate Γ_q quanta per second. Assume that the current $I_q = q\Gamma_q$ is stationary and that the flow events are uncorrelated. Then, for positive frequencies the single-sided spectral density of the flow rate is constant:

$$S_{\Gamma_q} = 2qI_q = 2q^2\Gamma_q,$$

with units of flow squared per hertz. (All the spectral densities written here are single-sided.) If photons from a coherent source with frequency $\nu > 2\Delta/h$ are absorbed in a detector at rate Γ_ν then the photon arrival times are uncorrelated, the quantum is one photon, and the spectral density of the absorbed photon flux is $S_{\Gamma_\nu} = 2\Gamma_\nu$.

Let $m \geq 2$ be the mean number of quasiparticles produced per absorbed photon so that $\Gamma_o = m\Gamma_\nu$ is the quasiparticle generation rate due to optical photons. The relationship between m and the pair-breaking efficiency η_{pb} is

$$m = \frac{\eta_{pb}P_A}{\Gamma_\nu\Delta} = \frac{\eta_{pb}h\nu}{\Delta},$$

since P_A/Δ would be the generation rate if all of the power excited quasiparticles exactly at the gap. Again considering a coherent source, the spectral density of the generation rate due to absorbed photons is

$$S_{\Gamma_o} = 2m^2\Gamma_\nu = 2m^2(\Gamma_o/m) = 2m\Gamma_o.$$

Two quasiparticles recombine per event, so the spectral density of the recombination rate Γ_R is

$$S_{\Gamma_R} = 2(2)^2(\Gamma_o/2) = 4\Gamma_o.$$

In steady state, the recombination rate due to optically excited photons equals the optical generation rate. (If optically excited quasiparticles dominate then we can also neglect recombination due to other excitation sources.) We see that if $\Gamma_o = \Gamma_R$ then $S_{\Gamma_o}/S_{\Gamma_R} = m/2$. In this work $m = 2$, so the generation noise from a coherent optical source equals the recombination noise due to the quasiparticles it excites.

To connect the above spectral densities to NEP referenced to a given point in an optical system, relate Γ_o to incident power P at that point:

$$P = \frac{P_A}{\eta} = \frac{h\nu\Gamma_\nu}{\eta} = \frac{h\nu\Gamma_o}{m\eta},$$

where $P_A = \eta P$. Referencing S_{Γ_o} to incident power gives

$$\text{NEP}^2 = \left(\frac{h\nu}{m\eta}\right)^2 S_{\Gamma_o} = \frac{2h\nu P}{\eta},$$

which matches the shot noise term in Equation 4 if the reference point is the source output. Referencing the recombination noise to incident power in the same way gives

$$\text{NEP}_R^2 = \left(\frac{h\nu}{m\eta}\right)^2 S_{\Gamma_R} = \frac{2}{m} \frac{2h\nu P}{\eta}.$$

Using η_{pb} instead of m gives

$$\text{NEP}_R^2 = \frac{4\Delta P}{\eta_{pb}\eta},$$

which matches Equation 5 if multiplied by η^2 to reference to absorbed power. The photon NEP of a chaotic source will also include a wave noise term, but this does not affect the conclusion that, in this work, the photon shot NEP term equals the NEP due to recombination from quasiparticles excited by that source.